15TH IEA HEAT PUMP CONFERENCE
MAY 26–29, 2026 | HOFBURG
VIENNA 2026
DECARBONISATION THROUGH INNOVATION

Compact, modular plug & play building heat pump using automotive components

Fynn Linnenbrügger[a,*], Jonas Hielscher[a], Jona Hauska[b], Zeinab Aghaziarati[c], Andreas Schulte[a], Lukas Radomsky[b], Wilhelm Tegethoff[a], Nicholas Lemke[a], Regine Mallwitz[b]

[a]Technische Universität Braunschweig, Institut für Thermodynamik, Hans-Sommer-Straße 5, Braunschweig 38106, Germany
[b]Technische Universität Braunschweig, Institut für Elektrische Maschinen, Antriebe und Bahnen, Hans-Sommer-Straße 66, Braunschweig 38106, Germany
[c]Institut für Solarenergieforschung Hameln (ISFH), Am Ohrberg 1, Emmerthal 31860, Germany

Abstract

This paper introduces a modular plug & play heat pump concept designed to address key challenges in the decarbonization of residential buildings, particularly in multi-family homes where conventional heat pump systems often face spatial, acoustic or infrastructural limitations. The concept builds scalable system architecture and standardized components from automotive thermal management, offering compactness, reduced refrigerant charge and potential for low-cost deployment. In addition, the early integration of a fault detection and diagnostics (FDD) system and the direct integration of power electronics for compressor drive and supply are introduced as part of the heat pump design process, in order to underline the holistic design approach.
Based on the presented heat pump concept the paper focuses on two main aspects. First, experimental measurements of key preliminary automotive components are conducted under typical building boundary conditions to show the general suitability for stationary heat pump application. Second, a model-based design methodology is introduced to determine the optimal heating capacity of a standardized module as well as component sizes by combining clustered weather data, annual heating load profiles and a numerical heat pump model. The compressor displacement is identified as a key design parameter and the proposed methodology enables an objective evaluation of how deviations from the optimal sizing affect annual energy performance. The findings underline the feasibility of the approach and provide a foundation for further optimization.

Keywords:Heat pump; Automotive components; Fault detection and diagnostics (FDD); Power electronics; Measurement results; Model-based heat pump design

1. Introduction

The decarbonization of the heating sector, particularly the replacement of fossil fuel-based heating systems in multi-family buildings, represents one of the major challenges on the path toward a climate-neutral building stock. In this context, heat pumps are widely regarded as a key enabler, offering a widely deployable solution for the provision of low-carbon heat. However, for multi-family buildings, their deployment is still limited. Existing heat pump solutions are typically centralized systems, which often face spatial, acoustic, technical or regulatory constraints during integration into complex existing building infrastructures. Moreover, apartment-based solutions are not yet standardized and widely available at scale. As a result, a technological gap persists between the theoretical potential of heat pumps for large scale decarbonization and their practical applicability in dense urban environments and heterogeneous building stocks.

To address these challenges, the research platform “Heat” within the research program “Transformation des Energiesystems Niedersachsen” (TEN.efzn) investigates a novel concept of a compact, modular plug &

* Corresponding author. Tel.: +49 (0)531 391 - 2632
E-mail address: f.linnenbruegger@tu-braunschweig.de

15th IEA Heat Pump Conference 2026 - ICO8.3 - https://doi.org/10.23697/t722-7d74

play heat pump module, utilizing of-the-shelf components derived from automotive thermal management. The core idea includes a standardized and scalable heat pump system architecture in which individual compact modules can be flexibly combined – analogous to the modular stacking principle of battery storage systems – to meet various heating demands. This modular approach enables broad applicability. In urban areas, a single module can provide heat for an individual apartment, even where conventional centralized air-to-water systems are infeasible due to noise or installations restrictions. In rural areas or less space-constrained environments, multiple modules can be combined into a "heat pump stack" to achieve higher heating capacities suitable for detached buildings.

The research primarily focuses on a water-to-water heat pump module, which can utilize multiple heat sources such as air via an additional air-to-brine heat exchanger, geothermal probes, groundwater or "cold" district and local heating. The concept allows integration into already existing district heating infrastructure by enabling a reduction of flow temperature. Hybrid configurations using air as a heat source via a secondary water/glycol circuit are being researched to extend applicability of the modular system. In the first step, the heat pump only has to provide room heating to collect experience. Further into the project, the use case will be expanded to also integrate domestic hot water provision.

Recent and ongoing research efforts investigated the general technical feasibility of compact heat pump systems and the utilization in multi-family homes. The Fraunhofer Institute for Solar Energy Systems (ISE) demonstrated within the "LC 150" research project that heating capacities of approximately 10 kW at 0 °C brine temperature and flow temperatures between 24 °C and 35 °C can be achieved with less than 150 g of R290 refrigerant, highlighting the potential low-charge propane heat pump systems [1]. Building upon these results, the ongoing "LC R290" project at Fraunhofer ISE focuses on the research of a compact propane heat pump system designed as a direct replacement for gas boilers in multi-family homes [2]. Similarly, the Austrian Institute of Technology (AIT) in collaboration with Ochsner Wärmepumpen GmbH explores drop-in propane heat pump concepts for larger multi-family homes within the "Gasthermenersatz" research project [3].

On the heat pump market, several products targeting apartment-level heating have recently emerged. The start-up HeatPump23 has introduced two small apartment air-to-water heat pump solutions with heating capacities of 6 kW and 9.5 kW at 7 °C air inlet temperature and 35 °C flow temperature utilizing R32 as refrigerant [4]. Similarly, Quantum Energy Technology ltd offers a 6 kW propane water-to-water propane heat pump module [5], while REMKO GmbH & Co. KG provides a compact apartment heat pump with a nominal heating capacity of 3 kW using R410a [6]. In addition, the Kensa Group provides a compact R134a heat pump with nominal heating capacities of 3 kW and 6 kW at a brine inlet temperature of 0 °C and flow temperature of 35 °C [7]. However, to date existing solutions do not combine modular scalability and the use of natural refrigerants, which is required for widespread and future-proof deployment in multi-family and single-family building configurations.

A key innovation of the present research project lies in transferring highly standardized automotive thermal-management components to residential heat pumps. Automotive components are characterized by compact design, high reliability and high dynamic performance range. These attributes suggest potential advantages in terms of adapting control strategies under typical building operating conditions. In addition, the durability of the components must be investigated, as they are not especially designed for stationary applications. In particular the number of on-off-cycles and on time of the automotive compressor will be analyzed. Due to the compact components of refrigerant cycles in automotive applications, there is also the potential to use easier oil management solutions compared to domestic heat pumps. Furthermore, the compact design constraints of automotive components offer promising opportunities for reducing refrigerant charge below 150 gram per module, enabling safe indoor installation in accordance with current safety standards [8]. Moreover, from a cost perspective the automotive industry provides mature supply chains and high volume production capacity, which may lead to low-costs and rapid procurement of components.

In addition to the different hardware concept, the integration of fault detection and diagnostics (FDD) functionality directly into the modular system architecture is considered from the early design phase. This ensures reliable and efficient operation, as even minor deviations from normal operation can reduce efficiency, shorten component lifetime, increase maintenance demands and compromise user safety. FDD allows for the early identification of typical fault conditions either through targeted experiments, numerical simulations or both. In heat pump systems, faults may originate from various mechanical, thermal or control-related causes and often develop gradually during operation. Previous studies [9], [10] have shown that faults are common across nearly all subsystems of heat pumps and can have a significant impact on performance if left unaddressed. Common faults include compressor degradation and failures [11], refrigerant charge deviations [12], leakage [12], fouling and corrosion of heat exchangers [12], malfunctioning expansion valves [13], sensor drift and calibration errors [14] as well as failures in secondary circuits [13]. As part of the project, further investigations will be carried out to determine how these faults can be reproduced either through experiments or numerical simulations in order to reliably identify and predict faults that occur during heat pump operation before they lead to system failure.

Within the holistic heat pump design process, the power electronics driving and supplying the compressor represent an important subsystem. Consequently, one key research area is integrating the compressor, its integrated inverter, and the power factor correction (PFC) rectifier directly into the heat pump housing. This functional integration enables optimal matching between the power electronics and compressor characteristics, improving energy efficiency and reducing system volume compared to separated solutions. To realize such integration, novel power electronic configurations and PFC-rectifier topologies are investigated.

For the implementation of a compact and modular system comprising power electronics and a compressor, several system-level configurations are feasible. One approach would be individual modules, consisting of a PFC rectifier, an intermediate direct current (DC)-link, and a compressor, as illustrated in Fig. 1a. This allows the PFC to be optimized for a single compressor, with the option to add or remove modules as needed. Alternatively, the system can employ a shared intermediate DC link, as shown in Fig. 1b, which enables higher-level control to selectively operate power electronic converters under partial load, thereby improving efficiency. However, additional diodes would be required to prevent current flow between PFC units [15], potentially increasing losses. A third approach utilizes a high-power three-phase PFC supplying multiple compressors, as depicted in Fig. 1c. While this concept reduces the number of required PFC rectifiers, it may result in an oversized system when operating only part of the compressors. Considering the power demand of the selected compressor and the overall goal of minimizing system complexity, the implementation approach utilizing individual modules is identified as most promising.

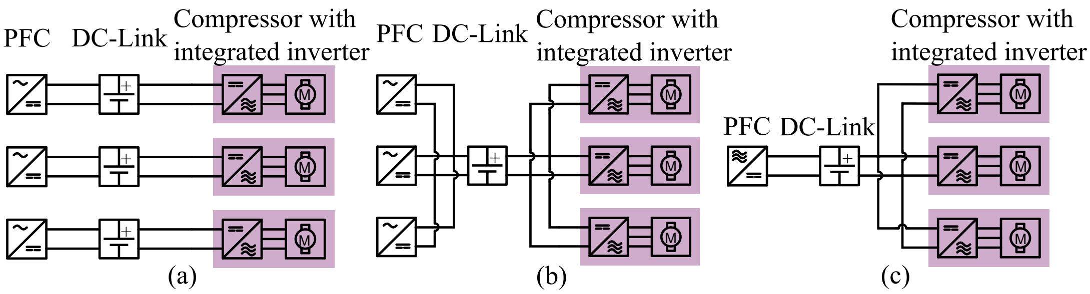

Figure 1. Conceptual block diagrams of the considered implementation approaches for the PFC-rectifier of the heat pump compressor

Further research will investigate various PFC rectifier topologies for the selected approach through a combination of numerical simulations and analytical calculations in order to identify optimal solutions for stationary heat pump applications. The simulation and calculation results will subsequently be validated by experimental investigations, first on the standalone power electronics prototype and subsequently through their integration into a compact heat pump test bench.

This paper presents a first conceptual overview covering multiple aspects of the modular plug & play heat pump system. Firstly, the feasibility of utilizing automotive-grade components for residential heat pump applications is evaluated and supported by initial experimental measurements of selected key preliminary components. Afterwards, a model-based design methodology for determining the optimal heating capacity for an individual heat pump module including the design of the key components is introduced. First design results based on generic simulation data are presented to demonstrate the applicability of the approach.

2. Measurement results of the automotive components

Initial experimental measurements were conducted using of-the-shelf components to assess the suitability of automotive thermal-management components for residential heat pump applications and to evaluate their performance under real world building operating conditions, which may differ significantly from the boundary conditions typical of automotive systems. The tested components include a 34 cm^3 scroll compressor and two Offset-Strip-Fin heat exchangers, serving as condenser and evaporator, both originated from current battery-electric vehicle platforms of German automotive manufacturers. The electric expansion valve was selected to match the system requirements, although it is not particularly designed for or used in automotive applications explicitly.

All experiments were carried out on a dedicated heat pump test bench at the facilities of TLK-Thermo GmbH, enabling both individual component characterization and system-level performance evaluation. Temperatures and pressures at the inlet and outlet of each component were recorded, along with the refrigeration mass flow rate and oil circulation rate. In the secondary circuits (heat source and sink), the inlet and outlet temperatures as well as volume flow rate were monitored. Due to the measurement of the oil circulation rate, an additional subcooler behind the condenser is installed.

The refrigeration cycle operates with propane as the working fluid. The measurement equipment used, including corresponding sensor ranges and uncertainties, is summarized in Table 1. In addition to the listed instruments, the uncertainties introduced by the data acquisition chain must also be considered. Two separate data acquisition system were employed. Thermocouples were connected to an analog input module with a gain error of ± 0.14 % of reading and ± 0.02 % of full scale. All other sensors were connected to a second analog input module with a gain error of ± 0.03 % of reading and ± 2 µV of full scale. A detailed uncertainty propagation analysis was conducted but is not presented here for brevity.

Table 1. Measurement ranges and uncertainties of used instruments

Parameter	Sensor	Range	Uncertainty
Refrigerant and secondary circuit temperatures	Thermocouple Type K, class 1	-40-375 °C	± 1.5 K of reading
Refrigerant pressure	Piezoresistive measuring element	0-2.5 MPa	± 0.25 % of full scale
Refrigerant mass flow rate	Coriolis mass flow meter	0-1202 kg/h	± 0.25 % of reading
Refrigerant-side pressure loss (evaporator)	Metal membrane	0-0.3 MPa	± 0.15 % of reading
Refrigerant-side pressure loss (condenser)	Metal membrane	0-0.3 MPa	± 0.05 % of reading
Oil circulation rate	Inline sound velocity sensor	0-10 wt%	± 0.4 % of reading
Heat source circuit volume flow rate	Magnetic-inductive flow sensor	0-40 l/min	± (0.8 % of reading + 0.5 % of full scale)
Heat sink circuit volume flow rate	Magnetic-inductive flow sensor	0-40 l/min	± 0.05 % of reading

All measurements presented here were conducted at oil circulation rates between 3 % and 5 %, with all derived quantities corrected for oil content effects. The tested operating range reflects typical boundary conditions for residential heat pump applications. The heat source circuit, using a water/glycol mixture featured inlet temperatures between -10 °C and 15 °C as well as temperature differences between inlet and outlet of 3 K to 10 K. The heat sink circuit exhibited water inlet temperatures ranging from 30 °C to 70 °C, with outlet temperature rises of approximately 4 K to 15 K.

Fig 2. presents the compressor map obtained from experimental measurements on the test bench. The x-axis represents the refrigeration suction volume flow rate, while the y-axis indicates pressure ratio. Each operating point is color coded according to the isentropic efficiency derived from the measured refrigerant outlet temperature of the compressor and an isentropic compression as a comparative process (see Eq. 4). Brighter colors denote higher isentropic efficiencies and darker colors lower ones. Dashed contour lines correspond to the compressor speed. The compressor operates within a speed range of 800 1/min up to 8500 1/min, achieving refrigerant volume flow rates between roughly 0.2 l/s and 4.7 l/s and pressure ratios between 2 and 11.

Overall, the compressor map reveals that low compressor speeds, corresponding to small suction volume flow rates, result in comparatively low isentropic efficiencies of around 35 % to 40 %. This reduction may be attributed to insufficient oil lubrication at low refrigerant volume flow rates. Similarly, for a given compressor speed, increasing pressure ratios lead to declining isentropic efficiencies, which could be explained, for example, by pressure conditions inside the chambers of the scroll spirals that deviate from the design conditions. This is supported by approximately equal isentropic efficiencies at a pressure ratio of 4 across all listed compressor speeds.

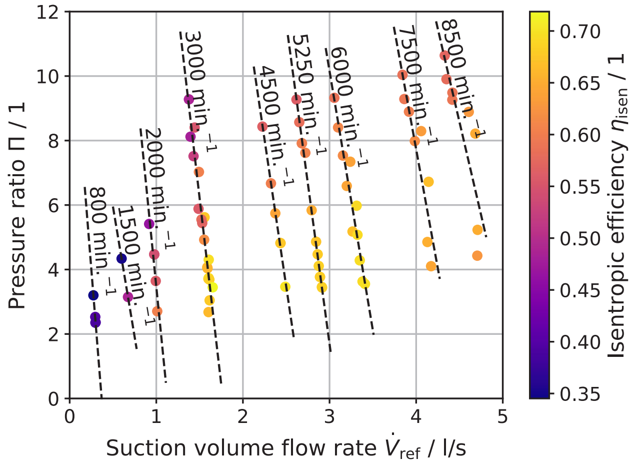

Figure 2. Compressor map resulting from the measurements, showing the isentropic efficiency as a function of pressure ratio and volume flow rates.

Fig. 3 shows the measurement results for the evaporator and condenser. In both diagrams, the *x*-axis displays the transferred heat flow, while the *y*-axis shows the resulting mean temperature difference (MTD) inside the heat exchanger. The dashed lines denote linear regressions describing the heat transfer capability as a function of MTD. To derive the MTD, each heat exchanger was discretized into a finite number of temperature-difference segments. The MTD is then calculated for each segment and the overall mean value is obtained from the segment distribution according to

$$\Delta T_{\mathrm{m}} = \frac{\dot{Q}}{\sum \Delta \dot{Q} / \Delta T} \quad . \tag{1}$$

The results for the evaporator show relatively large MTD's of approximately 5 K to 7 K even at low heat transfer rates. This behavior corresponds to a comparatively low heat transfer capability (*kA*-value) of about 410 W/K, resulting in MTD values up to 15 K at transferred heat rates of around 6.5 kW. In contrast, the condenser exhibits a significantly higher heat transfer capability of approximately 1230 W/K. Consequently, the derived MTD values are much lower, ranging from about 1.7 K at 1.2 kW to 9 K at 10 kW of transferred heat flows.

In summary, the condenser demonstrates suitable thermodynamic characteristics and heat transfer performance for the investigated operating range. However, the evaporator appears to be under-dimensioned, as indicated by its comparatively low heat transfer capability and the resulting higher temperature differences.

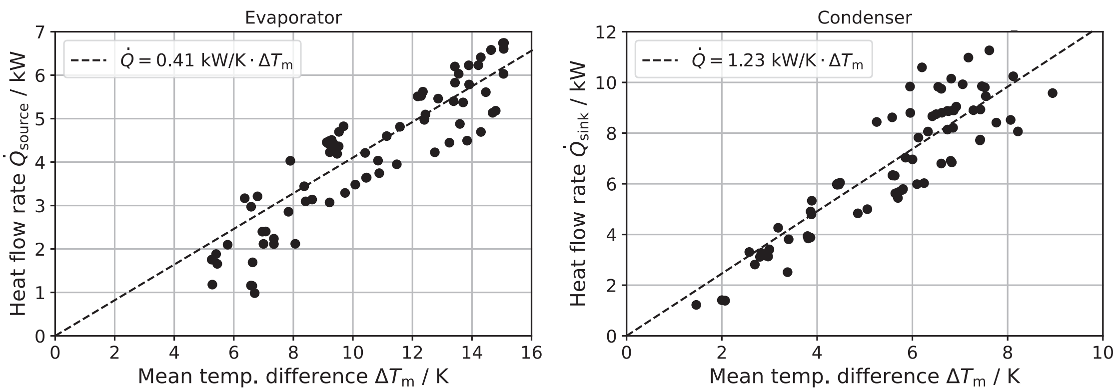

Figure 3. Transferred heat flow as a function of the mean temperature difference for the used evaporator and condenser.

3. Model-based design approach for heat pumps

In conventional heat pump development, manufacturers typically offer a series of products with different nominal heating capacities to address various building types and heating demands. In contrast, the proposed modular plug & play heat pump concept aims to research a single standardized module with a defined nominal heating capacity, enabling different total outputs by combining multiple identical modules. Consequently, determining the optimal heating capacity for an individual module and appropriately designing its key components represent a challenging task. Addressing this, the novel model-based heat pump design approach introduced in this work provides a systematic methodology to identify the optimal module configuration and heating capacity. The general workflow starts with the use of weather data to generate annual heating load profiles. These profiles and the weather data are then used as boundary conditions for the numerical heat pump model. The model is used to compute annual hourly based duration curves and to derive performance indicators such as energy consumption or cost. By iteratively adjusting the component parameters within the model, an optimization process is performed until the most suitable configuration is obtained. The overall concept and methodological steps of the model-based design approach are illustrated in Fig. 4.

The first step (1) focuses on the preparation and utilization of weather data. This weather data will be used to generate annual heating load profiles (3) through TRNSYS [16] (2) and serves as a boundary condition for the heat pump model (4) if air is used as a heat source. Typically, in engineering practice and building simulations related to the design of heating and cooling systems, the 15 Test Reference Year (TRY) regions are commonly used. This standardized weather dataset divides Germany into 15 climatic regions with similar weather characteristics. Each TRY region represents a contiguous geographic area, even though weather patterns and boundary conditions for the design and operation of heat pumps can be comparable across non adjacent regions and may also differ within a climate region. Therefore, 13 new clusters from the TRY2017 dataset will be identified to represent regions with similar boundary conditions for an air sourced heat pump. Each cluster will be represented by a location that best reflects the average boundary conditions within that cluster.

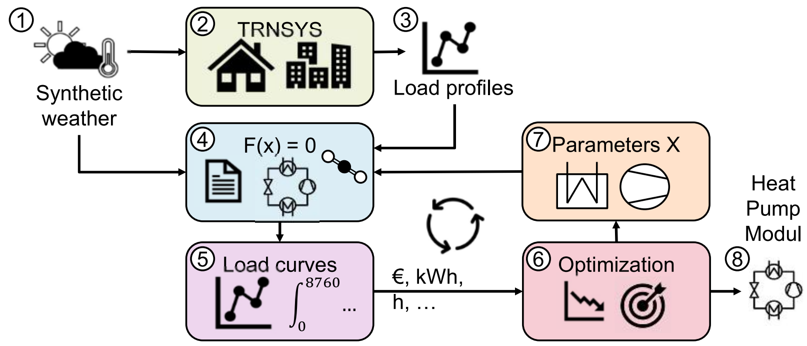

Figure 4. Graphical visualization of the different steps within the model-based heat pump design approach consisting of preparation and utilization of weather data, generation of heating load profiles through TRNSYS, simulation of the heat pump and optimization of key performance indicators (KPIs).

The newly selected weather data representing each cluster will then be utilized to generate load profiles (3) from a dynamic building model within TRNSYS (2) by the project partner siz energieplus, based on the defined uses cases [17]. In contrast to the standardized heating load calculation commonly used in practice in accordance with DIN EN 12831-1:2017-09 [18], which assumes static boundary conditions and design temperatures, the use of time-resolved weather data enables the determination of actual dynamic heating loads as well as their annual frequency distribution in relation to the corresponding outdoor temperature and the buildings thermal characteristics.

By combining the weather profiles (1) of each reference point with the respective annual heat load profile (3) as boundary conditions for a static heat pump model (4), annual duration curves and heat pump operating profiles are obtained (5). These results form the basis for a demand-based heat pump and component design. For instance, reducing compressor displacement may decrease the annual coverage of the heating energy demand but can extend system lifetime by lowering the number of on-off-cycles due to improved partial load behavior.

The numerical heat pump model (4) is based on a simplified vapor-compression cycle consisting of four main components: compressor, condenser, expansion valve and evaporator. Advanced cycle configurations with an internal heat exchanger are not covered in this paper, but will be looked at in the future.

Thermophysical fluid properties of the refrigerant propane are calculated using TILMedia Suite [23][24] (Version 2025.1) from TLK-Thermo GmbH, enabling the calculation of the relevant properties at the respective thermodynamic state points before and after each component. Flow-related pressure losses in the heat exchangers are neglected in this paper. In this study, the compressor is represented by a model with constant isentropic, effective isentropic and volumetric efficiencies (η_{isen}, $\eta_{\mathrm{isen,eff}}$ and λ). The mass flow rate imposed by the compressor $\dot{m}_{\mathrm{ref}}$ is calculated as a function of refrigerant density ρ_{ref} at the compressor inlet, the volumetric efficiency λ, compressor frequency n and compressor displacement V_{disp} (Eq. (2)).

$$\dot{m}_{\mathrm{ref}} = \rho_{\mathrm{ref,suc,comp}} \cdot \lambda \cdot n \cdot V_{\mathrm{disp}} \tag{2}$$

The power transported to the refrigerant P_{ref} is derived from the enthalpy difference between inlet and outlet refrigerant states (Eq. (3)), where the outlet enthalpy h_{out} is determined from the inlet enthalpy h_{in} and the specified isentropic efficiency η_{isen} in accordance to Eq. (4).

$$P_{\mathrm{ref}} = \dot{m}_{\mathrm{ref}} \cdot (h_{\mathrm{out}} - h_{\mathrm{in}}) \tag{3}$$

$$h_{\mathrm{out}} = h_{\mathrm{in}} + \frac{h_{\mathrm{out,isen}} - h_{\mathrm{in}}}{\eta_{\mathrm{isen}}} \tag{4}$$

The shaft power P_{shaft} represents the mechanical power required to drive the compressor. Any deviation between the shaft power and power transported to the refrigerant, which may be caused by friction losses, for example, is accounted for by a heat loss to the ambient $\dot{Q}_{\mathrm{amb}}$ (see Eq. 5). To demonstrate the applicability of this approach, it is assumed that there is no deviation between P_{shaft} and P_{ref}.

$$P_{\mathrm{shaft}} = P_{\mathrm{ref}} + \dot{Q}_{\mathrm{amb}} = \dot{m}_{\mathrm{ref}} \cdot \frac{h_{\mathrm{out,isen}} - h_{\mathrm{in}}}{\eta_{\mathrm{isen,eff}}} \tag{5}$$

Generally, the heat exchanger is based on a constantly specified heat transfer capability (*kA*-value) approach. The heat transfer is divided into a liquid phase, gas phase and vapor-liquid equilibrium region, as each region is assigned with a single cell. The transferred heat is calculated using Eq. 6 with the help of the thermodynamic mean temperature difference inside the heat exchanger, which is calculated with discretization into two (evaporator) or three (condenser) regions (see Eq. 1). The thermodynamic mean temperature inside one cell will be calculated using the logarithmic mean temperature due to low discretization.

$$\dot{Q} = k \cdot A \cdot \Delta T_{\mathrm{m}} \tag{6}$$

The correlation for the expansion valve is based on an isenthalpic change of state. Therefore, the refrigerant outlet temperature is calculated using the inlet enthalpy at the evaporating pressure.

To build an overall model for the refrigeration cycle two heat exchangers serving as the condenser and evaporator, a compressor and an expansion valve are connected together to form a simple vapor compression cycle. It is assumed that the superheating after the evaporator is identical with the temperature difference between the inlet and outlet temperatures of the heat source circuit. The subcooling at the condenser outlet is calculated to meet the pinch point inside the condenser. To incorporate air as a heat source with a secondary circuit, a reduction of the outdoor air temperature over the secondary circuit of 5 K is applied. This accounts for the temperature difference introduced by an additional air-to-brine heat exchanger. The flow and return temperature are derived by a heating curve to account for the dependency of the outdoor temperature.

The suitability of a heat pump configuration can be assessed based on several criteria, including annual delivered heating energy and electrical energy consumption to calculate the seasonal performance factor (SPF), total cost of ownership – comprising both investment and operating cost – as well as service life of the compressor, which can be evaluated through metrics such as the number of on-off-cycles and cumulative operating time. Depending on the selected combination of performance indicators (5), the respective quantities and decision variables are passed to an optimization framework (6). These variables are iteratively adjusted (7) according to a cost function formulated to reflect the specific design objective until an optimum configuration (8) is identified. In this manner optimal component dimensions and the heating capacity of a single heat pump module can be determined via multi objective optimization.

Table 2 summarizes the set parameters for the compressor, heat exchanger and overall refrigeration cycle used for the following described first design calculation. Parameters are based on market research into available components and engineering experience.

Fig. 5 presents the simulated annual thermal and electrical energy shares of the heat pump and auxiliary electric heater for two compressor displacements with values of 20 cm^3 (left) and 34 cm^3 (right), derived from annual duration curves. Each configuration comprises two plots in which the *x*-axis represents the cumulative annual operating hours. The upper diagrams depict the provided heating power, with the green area corresponding to the thermal energy provided by the heat pump and the red area to the thermal energy provided by the auxiliary heater. The lower diagrams show the respective electrical power consumption and resulting annual electrical energy shares. The instantaneous curve height represents the delivered or demanded power at a given time, while the area under the curve corresponds to the accumulated energy share over the year. The simulation over the span of a year is discretized in hourly time steps (up to 8760 steady state solutions) using representative German weather data provided by the Deutsche Wetterdienst (DWD) for Potsdam and employing the model parameters summarized in Table 2.

Table 2. Parameters for the numerical heat pump model

Parameter	Value
Minimal compressor frequency	800 1/min
Maximal compressor frequency	8500 1/min
Compressor displacement	20 or 34 cm^3
Isentropic efficiency	0.7
Effective isentropic efficiency	0.7
Volumetric efficiency	0.9
Evaporator brine inlet and outlet temperature difference	5 K
Condenser *kA*-value	1200 W/K
Evaporator *kA*-value	800 W/K

A comparison of both compressor displacements reveals that the larger 34 cm^3 compressor provides a significantly higher annual thermal energy share of 96 % than the smaller 20 cm^3 compressor with 78 %. Additionally, the smaller 20 cm^3 unit fails to cover the required heating load for approximately 2000 hours a year, as indicated by the red portions in the upper-left diagram, while the 34 cm^3 configuration requires auxiliary support only during around 800 hours a year. Overall, the maximum resulting heating demand of the used load profile is 13.8 kW, which cannot be provided by both heat pumps with different sizes. The system with the smaller compressor reaches thermal capacities of approximately 7 kW, whereas the heat pump with the 34 cm^3 compressors achieves 10 kW of thermal output. Consequently, the 20 cm^3 compressor can be considered undersized for the investigated boundary conditions, as the larger compressor more adequately covers the annual demand from a thermal performance perspective.

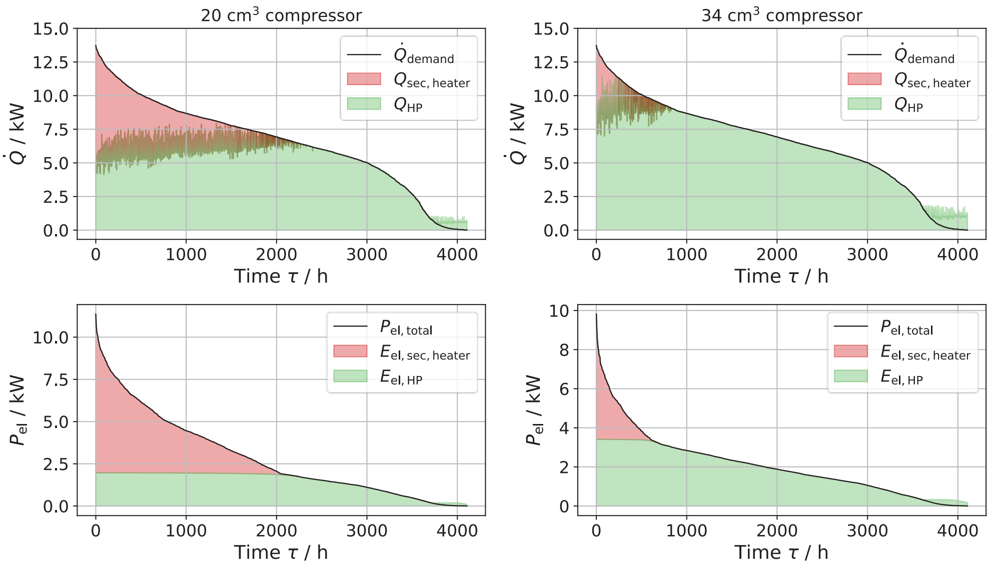

Figure 5. Visualization of the annual thermal and electrical energy share of the heat pump and auxiliary electrical heater, derived from the respective annual duration curves.

In addition, certain periods occur during the year in which the heat pump delivers more thermal power than required by the building load profile. For the 20 cm^3 compressor, this condition is observed for approximately 500 operating hours, when the minimum heating capacity of about 0.8 kW exceeds the heat demand. In the case of the 34 cm^3 compressor, this behavior extends to roughly 800 hours due to its higher minimum heating capacity of around 1.5 kW, resulting from the larger displacement, even though both compressors operate at the same minimum speed. During these periods, the system would operate in on-off-cycling mode, meaning that the compressor would not run continuously throughout each one-hour simulation interval. Such cycling operation negatively affects compressor lifetime and will therefore be explicitly considered in future component optimization and capacity sizing of an individual heat pump module.

The electrical power demand illustrated in the lower diagrams underlines these findings. Higher electrical power levels occur primarily during low ambient temperatures, coinciding with periods of elevated heating demand. As seen in the upper diagrams, the smaller compressor exhibits a considerably higher share of auxiliary heater operation, resulting in an increased electrical power demand and reduced system efficiency. Furthermore, its electrical power curve indicates operation at maximum compressor speed for nearly 50 % of the annual runtime, compared to only about 20 % for the 34 cm^3 compressor. This is indicated by the plateau behavior within the electrical power consumption, as the compressor power remains nearly constant after the heat pump reaches its maximum thermal output.

Moreover, when evaluating the SPF (Eq. 7) of the heat pump, the 20 cm^3 compressor heat pump has a SFP of 3.51, compared to 3.38 for the 34 cm^3 compressor heat pump. The small difference refers to the different heat flow rates of the heat exchangers. However, when extending the assessment to the overall system performance, including both the heat pump and auxiliary heater, the difference becomes more pronounced. In the smaller system, the auxiliary heater contributes a notably higher share of the annual electricity demand, resulting in a lower SPF on system level compared to the system equipped with a larger compressor (2.26 versus 3.09).

$$SPF_{\mathrm{HP}} = \frac{E_{\mathrm{el,HP}}}{Q_{\mathrm{HP}}} \quad \text{and} \quad SPF_{\mathrm{system}} = \frac{E_{\mathrm{el,HP}} + E_{\mathrm{el,sec,heater}}}{Q_{\mathrm{HP}} + Q_{\mathrm{sec,heater}}} \tag{7}$$

Efficiency variations depending on the compressor speed have not been implemented in the present model. Therefore, potential performance degradation at particularly low and high compressor speeds is not captured. Under the assumption of constant compressor efficiencies, the larger compressor predominantly operates under partial-load conditions. This might be advantageous based on the preliminary measurements. Overall, the results indicate that the 34 cm^3 configuration is more suitable, as the heat pump's electrical energy share is much higher than for the 20 cm^3 configuration. This would be reflected in the operating costs, since the efficiency of the heat pump itself is significantly better than that of the electric auxiliary heater, even under unfavorable operating conditions.

Although economic considerations and optimization of KPIs are not yet included in the model, the results demonstrate that the presented model-based approach is suitable for selecting the appropriate sizes of components and heating capacity for a single heat pump module based on heat load profiles.

4. Conclusion

This work introduces a compact, modular plug & play heat pump concept that leverages components from automotive thermal management. The proposed approach addresses key limitations of current residential heat pumps by combining compact component integration, a scalable system architecture and the direct integration of power electronics for driving the compressor directly within the heat pump housing. Furthermore, by incorporating FDD functionality, typical faults in residential heat pumps and their auxiliary systems can be identified at an early stage, enabling condition-based maintenance and increasing overall system reliability.

First experimental investigations using propane as refrigerant demonstrate that a refrigerant cycle based on automotive components can operate under typical residential boundary conditions. However, the measurements also indicate that the tested evaporator exhibits comparatively low heat transfer capability, suggesting that alternative component selection may yield notable efficiency improvements.

Initial results from the model-based design approach show that an appropriate choice of compressor displacement is essential to balance annual heating coverage and reliance on auxiliary heater operation without oversizing key components. In the examined exemplary cases with varied compressor displacement but constant compressor speed ranges, the heat pump system with the larger 34 cm^3 compressor demonstrates clear advantages in thermal performance, electrical energy consumption and seasonal system efficiency compared to a smaller sized heat pump system.

In the future, the model-based design framework will be extended to include a more complex compressor model, more detailed assessment of cycling behavior and economic optimization. Additional experimental investigations of further component variants will support systematic component selection in accordance to the results of the model-based design approach. The development of a dedicated test bench will help to demonstrate and validate the compact modular system design. Furthermore, the impact of varying the cycle topologies on the refrigerant charge, annual energy performance and compactness will be investigated.

Acknowledgements

The present is work is part of the Project “TEN.efzn – Transformation of the Energy System in Lower Saxony” which is funded by “zukunft.niedersachsen”, the joint science promotion program of the Lower Saxony Ministry of Science and Culture and the Volkswagen Foundation. The authors thank the ministry and project partners for funding and support. Responsibility is assumed by the authors for the content of this publication.

References

[1] Lena Schnabel, Katharina Morawietz, Timo Methler, Thore Oltersdorf, Hannes Fugmann, and Clemens Dankwerth, ‘LC150 – ENTWICKLUNG EINES KÄLTE-MITTELREDUZIERTEN WÄRMEPUMPEN-MODULS MIT PROPAN’, Fraunhofer ISE, Abschlussbericht. Accessed: Nov. 04, 2025. [Online]. Available: https://edocs.tib.eu/files/e01fb24/1887994033.pdf

[2] Fraunhofer ISE, ‘The LC R290 project’. Accessed: Nov. 04, 2025. [Online]. Available: https://lcr290.eu/project/lcr290/

[3] Gasthermenersatz’ project, ‘Gasthermenersatz - AIT Austrian Institute Of Technology’. Accessed: Nov. 04, 2025. [Online]. Available: https://www.ait.ac.at/themen/efficient-buildings-and-hvac-technologies/projekte/gasthermenersatz

[4] HeatPump23 GmbH, ‘Etagen-Wärmepumpe’. Accessed: Nov. 04, 2025. [Online]. Available: https://heatpump23.de/produktdetails

[5] Qvantum Energy Technology ltd, ‘Qvantum QGM – Apartment heat pump’. Accessed: Nov. 05, 2025. [Online]. Available: https://www.qvantum.com/uk/consumer-product/qvantum-qg®/

[6] REMKO GmbH & Co. KG, ‘Modulare Wärmepumpen ⇒ Serie MWL’. Accessed: Nov. 04, 2025. [Online]. Available: https://www.remko.de/neue-energien/modulare-waermepumpen/mwl/

[7] Kensa Group Limited, ‘Technical Information Sheet - Kensa Shoebox Heat Pump’. Accessed: Nov. 05, 2025. [Online]. Available: https://cdn.sanity.io/files/lnwa68k7/production/2d8d04b503383466bd52420b43b6f3a681c53f5a.pdf

[8] DIN Deutsches Institut für Normung e. V., *DIN EN 378-1: Kälteanlagen und Wärmepumpen – Sicherheitstechnische und umweltrelevante Anforderungen – Teil 1: Grundlegende Anforderungen Begriffe, Klassifikationen und Auswahlkriterien; Deutsche Fassung EN 378-1:2016+A1:2020*, Dec. 2020.

[9] I. Bellanco, E. Fuentes, M. Vallès, and J. Salom, ‘A review of the fault behavior of heat pumps and measurements, detection and diagnosis methods including virtual sensors’, *Journal of Building Engineering*, vol. 39, p. 102254, Jul. 2021, doi: 10.1016/j.jobe.2021.102254.

[10] B. Llopis-Mengual and E. Navarro-Peris, ‘Effects of simultaneous soft faults in a reversible and variable-speed air-to-water heat pump’, *Applied Thermal Engineering*, vol. 254, p. 123883, Oct. 2024, doi: 10.1016/j.applthermaleng.2024.123883.

[11] J. J. Aguilera *et al.*, ‘A review of common faults in large-scale heat pumps’, *Renewable and Sustainable Energy Reviews*, vol. 168, p. 112826, Oct. 2022, doi: 10.1016/j.rser.2022.112826.

[12] P. Barandier and A. J. Marques Cardoso, ‘A review of fault diagnostics in heat pumps systems’, *Applied Thermal Engineering*, vol. 228, p. 120454, Jun. 2023, doi: 10.1016/j.applthermaleng.2023.120454.

[13] Y. Guo, C. Du, Y. Wang, Y. Liu, and J. Zhu, ‘Experimental study on typical faults and operational performance analysis of carbon dioxide heat pump system’, *International Journal of Refrigeration*, vol. 170, pp. 349–362, Feb. 2025, doi: 10.1016/j.ijrefrig.2024.12.007.

[14] H. Madani and E. Roccatello, ‘A comprehensive study on the important faults in heat pump system during the warranty period’, *International Journal of Refrigeration*, vol. 48, pp. 19–25, Dec. 2014, doi: 10.1016/j.ijrefrig.2014.08.007.

[15] Jaehong Hahn, P. N. Enjeti, and I. J. Pitel, ‘A new three-phase power factor correction (PFC) scheme using two single-phase PFC modules’, in *APEC 2001. Sixteenth Annual IEEE Applied Power Electronics Conference and Exposition (Cat. No.01CH37181)*, Anaheim, CA, USA: IEEE, 2001, pp. 813–819. doi: 10.1109/APEC.2001.912463.

[16] Klein, S.A. et al., *TRNSYS 18: A Transient System Simulation Program*. (2017). FORTRAN. Solar Energy Laboratory, University of Wisconsin, Madison, USA. Accessed: Nov. 07, 2025. [Online]. Available: https://sel.me.wisc.edu/trnsys/

[17] F. Bockelmann *et al.*, ‘Implementation and use cases of a compact, modular heat pump for residential buildings’, presented at the 27th IEA Heat Pump Conference, Vienna, 2026.

[18] DIN Deutsches Institut für Normung e.V., *DIN EN 12831-1:2017-09, Energetische Bewertung von Gebäuden - Verfahren zur Berechnung der Norm-Heizlast - Teil 1: Raumheizlast, Modul M3-3; Deutsche Fassung EN 12831-1:2017*, Sep. 2017.

[19] Ingo Frohböse, ‘TILMedia Suite’. Accessed: Nov. 12, 2025. [Online]. Available: https://www.tlk-thermo.com/en/software/tilmedia-suite

[20] E. W. Lemmon, M. O. McLinden, and W. Wagner, ‘Thermodynamic Properties of Propane. III. A Reference Equation of State for Temperatures from the Melting Line to 650 K and Pressures up to 1000 MPa’, *J. Chem. Eng. Data*, vol. 54, no. 12, pp. 3141–3180, Dec. 2009, doi: 10.1021/je900217v.